HHS Public Access

Author manuscript

J Mol Biol. Author manuscript; available in PMC 2021 July 09.

Published in final edited form as:

J Mol Biol. 2021 July 09; 433(14): 166845. doi:10.1016/j.jmb.2021.166845.

Evolutionary Conservation of Structural and Functional Coupling between the BRM AT-Hook and Bromodomain

Brianna E. Lupo[1], **Peirou Chu**[1], **Michael J. Harms**[2,3], **Emma A. Morrison**[1,4], **Catherine A. Musselman**[1,5]

[1] - University of Iowa, Carver College of Medicine, Department of Biochemistry, Iowa City, IA 52242, United States

[2] - Institute of Molecular Biology, University of Oregon, Eugene, OR 97403, United States

[3] - Department of Chemistry and Biochemistry, University of Oregon, Eugene, OR 97403, United States

[4] - Medical College of Wisconsin, Department of Biochemistry, Milwaukee, WI 53226, United States

[5] - University of Colorado Anschutz Medical Campus, Department of Biochemistry and Molecular Genetics, Aurora, CO 80045, United States

Abstract

The BAF chromatin remodeling complex is critical for genome regulation. The central ATPase of BAF is either BRM or BRG1, both of which contain a C-terminal bromodomain, known to associate with acetylated lysines. We have recently demonstrated that in addition to acetyl-lysine binding, the BRG1/BRM bromodomain can associate with DNA through a lysine/arginine rich patch that is adjacent to the acetyl-lysine binding pocket. Flanking the bromodomain is an AT-hook separated by a short, proline-rich linker. We previously found that the AT-hook and bromodomain can associate with DNA in a multivalent manner. Here, we investigate the conservation of this composite module and find that the AT-hook, linker, and lysine/arginine rich bromodomain patch are ancient, conserved over ~1 billion years. We utilize extensive mutagenesis, NMR spectroscopy, and fluorescence anisotropy to dissect the contribution of each of these conserved elements in association of this module with DNA. Our results reveal a structural and functional coupling of the AT-hook and bromodomain mediated by the linker. The lysine/arginine rich patch on the bromodomain and the conserved elements of the AT-hook are critical for robust affinity for DNA, while the conserved elements of the linker are dispensable for

Correspondence to Emma A. Morrison and Catherine A. Musselman: Medical College of Wisconsin, Department of Biochemistyr, Milwuakee, WI 53226, United States and University of Colorado Anschutz Medical Campus, Department of Biochemistry and Molecular Genetics, Aurora, CO 80045, United States. emorrison@mcw.edu*(E.A. Morrison)*, catherine.musselman@cuanschutz.edu*(C.A. Musselman)*.

Declaration of Competing Interest

The authors declare that they have no known competing financial interests or personal relationships that could have appeared to influence the work reported in this paper.

Appendix A. Supplementary data

Supplementary data to this article can be found online at https://doi.org/10.1016/j.jmb.2021.166845.

overall DNA affinity but critical for maintaining the relative conformation of the AT-hook and bromodomain in binding to DNA. This supports that the coupled action of the AT-hook and bromodomain are important for BAF activity.

Keywords

AT-hook; bromodomain; chromatin; BAF complex

Introduction

The eukaryotic genome is packaged into the cell nucleus as chromatin, a complex between the DNA and histone proteins. In addition to considerably compacting the DNA, chromatin structure regulates all DNA-templated processes. As such, chromatin structure must be spatially and temporally remodeled throughout the life-cycle of the cell.[1] This is mediated in part by ATP-dependent chromatin remodeling complexes.[2–5] The BRG1/BRM associated factor (BAF) complex is one such complex, which is a part of the SWI/SNF family of remodelers. BAF contains up to 15 subunits that assemble in a combinatorial manner depending on cell type and developmental stage.[6,7] BAF is critical for mediating genome accessibility and is mutated in about 20% of all human cancers as well as in some neurological and developmental disorders.[7–12]

The ATPase subunit of BAF is either BRM (*Smarca2*) or BRG1 (*Smarca4*). Though they have high sequence similarity and similar *in vitro* activity, they form mutually exclusive complexes, are differentially expressed during development, and cannot substitute for one another *in vivo*.[13,14] BRM and BRG1 diverge in sequence most greatly in the N-terminal region, where transcription factors can associate, and are otherwise well conserved. Two recent cryo-EM structures of the BAF complex in association with a single nucleosome in the absence of ATP reveal that BRG1 and SMARCB1 sandwich the nucleosome, while the remaining components that are present support this architecture.[15,16]

A number of auxiliary histone and DNA binding domains (outside the DEXDc/HELICc ATPase core) are found throughout remodeling complexes. It has been proposed that in addition to providing general affinity for chromatin, these interactions could regulate activity in response to the local chromatin environment.[3] The unique combination of regulatory domains would thus lead to specialized function of each remodeler. In the BAF complex these auxiliary domains include an AT-hook and bromodomain (BD) at the C-terminus of BRG1/BRM, separated by a 6-amino acid linker (Figure 1A). The BRG1/BRM BDs have been shown to bind acetylated histone tails.[17–19] In addition, we have recently shown that these BDs can bind to DNA.[19,20] BD binding to DNA is enhanced by the adjacent AT-hook, an intrinsically disordered DNA-binding motif. We found that this multi-component module has moderate preference for AT-rich DNA and that the AT-hook and BD span the minor and major grooves respectively.[20] These regions do not resolve in the recent BAF/nucleosome structures, but based on the position of the BRG1 C-terminus would clearly be positioned at the nucleosome interface near the H3 tail and entry DNA.[15,16] This suggests that they

directly associate with the nucleosome substrate, however, the importance of DNA binding by the AT-hook and BD in BAF function has yet to be determined.

To further investigate the importance of this motif in BAF activity, we studied its evolutionary origin and conservation. We found that the AT-hook, the linker, and the lysine/arginine rich patch on the BD evolved nearly one billion years ago and have been conserved in most animal lineages. Through extensive mutagenesis, we determined the relative contribution of these conserved regions to the DNA binding activity and the conformational integrity of the DNA-bound state. We found that the AT-hook, linker, and BD are structurally and functionally coupled in binding to DNA. Conserved residues in the AT-hook and BD make critical direct contacts with DNA, while conserved residues in the linker are dispensable for overall affinity but promote a unique bound state. Notably, many of the strongly conserved residues are mutated in cancer. Together this suggests the importance of this coupled DNA binding activity in BAF function.

Methods

BRM constructs

In these studies AT-L-BD corresponds to the AT-hook, linker, and bromodomain from an alternatively spliced variant of BRM (known as BRM-B). This corresponds to residues 1358–1399 + 1418–1508 of UniProtKB entry P51531, which lacks an internal loop (residues 1400–1417) that we have previously shown does not contribute to DNA binding.[19] This construct was cloned from a codon-optimized gene block of the BRM-A spliceoform residues 1358–1508 that was obtained from Integrated DNA Technologies (IDT) and cloned into the pDEST15 vector using Invitrogen Gateway recombination technology (ThermoFisher Scientific). The BRM AT-hook (residues 1358–1377, referred to as AT here) was also generated from this plasmid using the Q5 site-directed mutagenesis kit (New England Biolabs). The N-terminal side of all constructs has an engineered PreScission Protease site allowing cleavage from the GST-tag. The following BRM mutants of the BRM-B AT-L-BD construct were additionally generated using the Q5 site-directed mutagenesis kit: AT_{GAGGG}-L-BD, AT_{GGGP}-L-BD, AT_{DGDP}-L-BD, AT-L_{PAPP}-BD, AT-L_{ANAA}-BD, AT-L-$BD_{3R/K\text{-}DNA}$, AT-L-$BD_{3R\text{-}D}$.

BL21 (DE3) Chemically Competent *Escherichia coli* cells (ThermoFisher Scientific and New England BioLabs) were used for expression of all constructs. Bacterial cultures were grown in LB media or M9 minimal media supplemented with vitamin (Centrum Daily), 1 g/L $^{15}NH_4Cl$, and 5 g/L D-glucose to generate ^{15}N-labelled protein. Cultures were grown to an OD of ~0.9–1.0 and induced using 0.3 mM IPTG at 18 °C for 16–20 h.

To purify the GST-tagged proteins, cells were lysed via sonication (Misonix Sonicator XL2020) in 20 mM Tris pH 7.5, 500 mM KCl, 3 mM DTT, 0.5% Triton X-100, 1 mg/mL lysozyme, protease inhibitor tablets (Roche), and DNaseI (Sigma). The soluble lysate was incubated with glutathione agarose resin (ThermoFisher Scientific) for ~1.5 h and washed with buffer (50 mM KPi pH 7.0, 50 mM KCl, 0.5 mM EDTA, and 1 mM DTT). The GST tag was cleaved with PreScission Protease overnight and further purified using cation exchange and size exclusion chromatography (Source 15S and Superdex 75 30/100, GE

Healthcare Life Sciences). The final buffer for all samples was 50 mM KPi pH 7.0, 50 mM KCl, 0.5 mM EDTA, and 1 mM DTT.

Urea denaturation and protein refolding

The WT and mutant constructs express with varying levels of monomeric and misfolded or aggregated forms of the construct. Growths that generated high yields of protein aggregate were dialyzed into buffer containing 3 M Urea, 50 mM KPi, 50 mM KCl, 0.5 mM EDTA, and 1 mM DTT for ~16 h at 4 °C and subsequently dialyzed into buffer containing 50 mM KPi, 50 mM KCl, 0.5 mM EDTA, and 1 mM DTT for 12–48 h at 4 °C. Following this re-folding, the protein was repurified via size exclusion chromatography. This procedure resulted in conversion from the aggregated form to the monomeric form, as evidenced by size exclusion elution profiles (see Figure Supplementary figure 2). An overlay of ^{1}H-^{15}N HSQC spectra collected on versions of the protein that were initially expressed and purified as a monomer versus partially denatured and refolded into monomeric form shows that the AT-L-BD construct refolds properly with this procedure (data not shown).

Concentration determination

Concentration of AT-L-BD constructs was determined using absorbance at 280 nm and calculated extinction coefficients. Concentration of the AT-hook construct was determined using the Pierce Quantitative Fluorometric Peptide assay (Thermo Scientific, product 23290).

DNA samples

DNA for use in the NMR studies was obtained from Integrated DNA Technologies with a sequence of 5′- CTCAATTGGT – 3′ and 5′ – ACCAATTGAG- 3′. Double stranded oligonucleotides were annealed by heating to 94° C for 10 min before being slowly cooled to room temperature. Annealed duplexes were purified by size exclusion chromatography (Superdex 75 30/100, GE Healthcare Life Sciences) in buffer (50 mM KPi, 50 mM KCl, 0.5 mM EDTA, 1 mM DTT, pH 7.0) and concentrated. Concentration was determined using absorbance at 260 nm and calculated extinction coefficients for dsDNA.

For use in Fluorescence Anisotropy studies, HPLC-purified 5′-fluorescein-labelled DNA oligos and unlabeled complimentary strands were obtained from IDT and annealed as described above. To ensure that the dsDNA was at least 99% hybridized at the low concentration used in FA experiments, the DNA sequence used for NMR experiments were extended by 2 bp to produce DNA.FA (5′−6-FAM-CCTCAATTGGTC-3′) and (5′-GACCAATTGAGG-3′).

NMR spectroscopy and data analysis

DNA titrations were carried out by collecting ^{1}H-^{15}N HSQC spectra on a given ^{15}N AT-L-BD construct in the apo state and with increasing concentrations of DNA. Protein samples were ~100 μM in 50 mM KPi pH 7.0, 50 mM KCl, 0.5 mM EDTA, and 1 mM DTT, and 10% D_2O. Assignments were transferred to mutant constructs by comparison to wild-type. Residues whose assignments could not be transferred with confidence were excluded from analysis and are marked as such. Titrations were collected at the following ratios of BRM

construct:DNA: WT AT-L-BD – 1:0, 1:0.25, 1:0.5, 1:1, 1:3, 1:6; AT –1:0, 1:0.25, 1:0.5, 1:1, 1:3, 1:6, 1:12, 1:19; AT_{GAGGG}-L-BD – 1:0, 1:0.25, 1:0.5, 1:1, 1:3, 1:6, 1:12, 1:20; AT_{GGGP}-L-BD – 1:0, 1:0.25, 1:0.5, 1:1, 1:3, 1:6, 1:12, 1:20; AT_{DGDP}-L-BD – 1:0, 1:0.25, 1:0.5, 1:1, 1:3, 1:6, 1:12, 1:20; AT-L_{ANAA}-BD – 1:0, 1:0.25, 1:0.5, 1:1, 1:3, 1:6; AT-L_{PAPP}-BD – 1:0, 1:0.25, 1:0.5, 1:1, 1:3, 1:6; AT-L-$BD_{3R\text{-}D}$ – 1:0, 1:0.25, 1:0.5, 1:1, 1:3, 1:6; 1:12, 1:20; AT-L-$BD_{3K\text{-}DNA}$ – 1:0, 1;0.1, 1:0.25, 1:0.5, 1:1, 1:3, 1:6; 1:12. Data were collected at 20 °C on an 800 MHz Bruker Avance II spectrometer with a TCI cryo probe. Titration data was processed in NMRpipe[21] and analyzed using Ccpnmr Analysis.[22]

The chemical shift difference (Δδ) for each point in the titration was calculated by $\Delta\delta = \sqrt{(\Delta\delta_H)^2 + (0.154\Delta\delta_N)^2}$ where δ_H and δ_N are the changes in the ^{1}H and ^{15}N chemical shift at each titration point with respect to the apo chemical shifts. K_d values were determined by fitting binding curves for residues with significant Δδs using a nonlinear least-squares analysis in GraphPad Prism 8. For AT alone, all residues were fit since all residues were perturbed in this short construct. Residues were considered to be significantly perturbed if the Δδ was larger than two deviations from the average Δδ value for all residues after trimming the largest 10% of values. Binding curves were fit to a single-site binding model under ligand-depleted conditions:

$$\Delta\delta = \Delta\delta_{max}\left(([L] + [P] + K_d) - \sqrt{([L] + [P] + K_d)^2 - 4[P][L]}\right)/(2[P])$$

where [P] is the concentration of protein, [L] is the concentration of DNA, $\Delta\delta_{max}$ is the chemical shift difference at saturation as compared to the apo state. K_d values are reported as the average and standard deviation of the fit K_d values for all significantly perturbed residues.

Fluorescence anisotropy

FA titrations were carried out using a Horiba Scientific Fluorolog-3 fluorimeter using FluorEssence software. Temperature was held at 20 °C using a water bath. Fluorescein-labelled samples were excited at 492 nm and emission was recorded at 515 nm with 5 nm excitation and emission bandpass. Anisotropy data were collected with 1 s integration time as an average of 10 values unless a 2% error tolerance was reached in fewer scans. G factors (I_{HV}/I_{HH}) were calculated for each point in the titration and were consistent across titrations. Anisotropy (r) is calculated as: $r = \frac{I_{VV} - GI_{VH}}{I_{VV} + 2GI_{VH}}$, where I_{VV} is the fluorescence emission intensity measured with vertically polarized excitation and vertically polarized emission. I_{VH} is the intensity measured with vertically polarized excitation and horizontally polarized emission. I_{HH} and I_{VH} are the intensity measure with horizontally polarized excitation and horizontally or vertically polarized emission, respectively.

Titration samples contained 100 nM 5′-fluorescein-labeled DNA in 50 mM potassium phosphate pH 7.0, 50 mM KCl, 0.5 mM EDTA, 1 mM DTT (for 129 mM total [K^+]) in a 3 mm quartz cuvette with initial volumes of 150 μL. Unlabeled BRM construct was titrated into the solutions. Binding curves were fit using nonlinear regression analysis in GraphPad

Prism 7 to a simple single-site binding model according to: $= r_0 + (r_{max} - r_0)\frac{x}{K_d + x}$ where r_0 is the anisotropy value for free DNA, r_{max} is the anisotropy value for the DNA-protein complex, x is the free concentration of protein (which is assumed to be equal to the total concentration of protein under assay conditions), and K_d is the dissociation constant. Titrations were collected in triplicate with binding affinities reported as the average and standard deviation of the fits to each individual titration.

Evolutionary analysis

We used BLASTp[23] to search for amino acid sequences of BRM and BRG1, aiming for broad taxonomic sampling across animals, plants, and fungi. We used the human protein sequences of BRM and BRG1 (Uniprot: P51531, P51532) for our initial search of animal proteomes, then used a broader set of animal BRG1/BRM sequences as search seeds for all other BRM and BRG1 sequences: *H. sapiens* P51531 and P51532, *G. gallus* Q90755 and Q90753, *D. rerio* Q7ZSY3 and XP_021332635.1, *P. marinus* XP_032826553.1, and *B. floridae* XP_019645515.1. We checked the orthology of each hit by reverse-BLAST against the human proteome. To achieve broad and relatively even taxonomic sampling, we performed multiple BLAST searches filtered by subphylum. We aligned our sequences using MUSCLE v3.8.1551.[24] We determined divergence times using TimeTree.[25] For the isoelectric point calculation, we extracted the sequence region corresponding to the ordered region of the bromodomain found in structure 2DAT. We estimated the isoelectric point of each species bromodomain using pdbtools (https://github.com/harmslab/pdbtools), which assumes model-compound pK_a values for all titratable amino acids. We calculated sequence logos using Weblogo 3 (http://weblogo.threeplusone.com/).[26] Our complete set of sequences, aligned AT-region, aligned bromodomain, and full alignment are given in Supplementary Table S1.

Results

The BRM AT-hook, linker and BD form an animal-specific module

We previously found that the BRG1/BRM AT-hook and BD form a composite DNA binding domain,[19,20] however the importance of this activity in BAF function is unclear. As conservation is a strong indicator of functional importance, we investigated the conservation of the DNA binding elements of this domain. In human BRG1 and BRM, this composite domain can be broken into three elements; the AT-hook, linker, and BD (see Figure Supplementary figure 1) The AT-hook contains the canonical RGRP central sequence flanked by K/R residues to the N-terminus and a K to the C-terminus, that are all involved in DNA binding. The linker between the AT-hook and BD is six amino acids and is proline rich, with a notable PNPP element just adjacent to the BD, the role of which in DNA binding not clear. Finally, the BD contains a K/R-rich patch in the αA helix and ZA-loop that is important in DNA binding. We investigated the evolution and conservation of each of these elements.

We first compared the AT-hook and linker regions from BRG1/BRM sequences sampled from 31 representative metazoan species (Supplementary Table S1), aiming for broad and even taxonomic sampling. A subset of these sequences is shown in Figure 1B. It appears that

Corals, which diverged from the human lineage ~695 million years ago,[25] differ from humans at only four of the 18 sites in this region. Even Trichoplax, which diverged ~930 million years ago, has obvious sequence similarity to the human sequence. The motif was not present, however, in the sampled sponge and choanoflagellate sequences. We therefore calculated a sequence logo for all of the sequences within ParaHoxozoa, the clade encompassing humans through Trichoplax (Figure 1C), which spans the AT-hook and linker. This reveals the strength of the conservation of both the AT-hook and linker for over 900 million years: there is a clear consensus pick for 16 of the 18 amino acids in this region.

To resolve when the AT-hook-linker motif evolved, we sampled the same region from 43 fungal and 36 plant BRM proteins. The sequence logos for these two clades are shown in Figure 1B. The fungal sequence has some similarity to the metazoan logo. Notably, the K/R residues preceding the RGRP are conserved across fungi and metazoans. In contrast, plants exhibit little conservation of these AT-hook regions, as revealed by their relatively flat sequence logo. This implies that the AT-hook and linker seen in humans evolved in two steps. First, the K/R-rich region preceding the RGRP evolved between 1.3 and 1.0 billion years ago, after the divergence of the animal/fungal lineage from plants, but before the divergence of animals and fungi. Next, the full AT-hook-linker motif (Figure 1C) evolved before the divergence that led Placozoa and Eumetazoa ~930 million years ago. The motif has since been maintained on many descendant Eumetazoan lineages, including humans.

We next investigated the evolution of the K/R-rich patch on the BD. The BD is found in all of the species studied. One key feature of DNA binding domains is a basic isoelectric point (pI), which allows them to interact favorably with the negative charge of the DNA phosphate backbone. We calculated the pI for all sequences in the dataset (see Figure 1B): as with the AT-hook and linker, a strong evolutionary pattern emerged. With the exception of *C. elegans*, all metazoan BDs have a basic pI (>7.0). In contrast, all non-metazoans have a BD with an acidic pI (<7.0). This suggests there may have been a functional transition for the BD around the time of the evolution of multicellular animals, in which it gained DNA binding activity.

We also looked at the conservation of specific sites in the BD including the K/R-rich residues (Figure 2A). We utilized consurf[27] to map the aligned HoxoPlacozoa BD sequences onto the previously solved structure of human BD (PDBID: 2DAT). Overall, there was a solvent exposed hydrophobic patch mixed with acidic residues that exhibited strong conservation and is known to be important for association with acetylated lysine (Figure 2B).[28] In addition, several hydrophobic core residues are conserved. Notably, few of the basic amino acids making up the K/R rich patch in the human BD exhibited strong conservation scores, because sites with R and K interchanged relatively freely over evolutionary time. The only exception to this was K1451. This may suggest that it is largely the overall charge, rather than sidechain-specific protein-DNA contacts, that is conserved. Notably, two Y residues in the ZA-loop, one of which we previously observed to form interactions in the major groove of DNA,[20] do show conservation.

Consistent with an early origin for this module, the region is highly similar across diverse species: for example, humans, acorn worms, horseshoe crabs, octopi, and corals all possess a basic stretch of amino acids followed by the RGRP, a PNPP element, and then a basic BD.

There have, however, been lineage-specific disruptions of this module. Notably, there appear to have been two, independent, disruptions of this pattern within the Ecdysozoa: within the flies (including *Drosophila*) and within the roundworms (including *Ceanorhabditis*). Both organisms have lost the AT-hook and surrounding elements. The *C. elegans* sequence has also acquired an acidic BD.

Interestingly, the majority of the species that lost one element in the module lost all of the elements: sea urchins, fruit flies, and round worms all lost essentially the whole motif—the AT-hook through the linker region. Termites are the only exception to this observation, having lost the PNPP element but maintained the AT-hook. Together this conservation, apparently as a module, may point to functionally important coupling between the module elements.

The AT-hook, BD, and linker are structurally coupled

To dissect the structural and functional coupling of each of these regions, we performed extensive mutagenesis in the AT-hook, linker, and BD in the context of the linked composite domain (AT-L-BD). Mutant constructs were generated for the K/R-rich and RGRP elements of the AT-hook, the linker, and the K/R-rich patch on the BD (see Figure 3 and Figure Supplementary figure 2). Together, this set of constructs allowed for a comprehensive investigation into the region-specific contributions to the affinity and mode of AT-L-BD DNA binding.

We first investigated the effect of these mutations on the conformation of the AT-L-BD using NMR spectroscopy. ^{1}H-^{15}N heteronuclear single quantum coherence (HSQC) spectra were collected on wild-type and mutant constructs (Figure Supplementary figure 1, Supplementary figure 3, Supplementary figure 4, Supplementary figure 5 and Supplementary figure 6). Differences in chemical shift (Δδ) were determined for mutant as compared to wild-type constructs to assess the effect of mutating individual regions on the conformation of the composite domain. Mutation of the AT-hook results in differences around the site of mutation with minimal to no differences in the linker or BD (Figure 4). Consistent with this, comparison of the HSQC spectra of the AT-L-BD with the AT-hook alone shows expected differences in peak intensity between the two constructs due to size and structural flexibility, but only chemical shift differences near where the AT-hook attaches to the linker (Figure 4 and Figure Supplementary figure 3). On the other hand, deletion of the AT-hook leads to differences in residues flanking where the AT-hook attaches to the linker as well as in the BD AB-loop (Figure 4).

Mutation of residues in the BD K/R-rich patch leads to localized chemical shift differences in the BD, while maintaining the overall BD fold (Figure Supplementary figure 6). Neither BD mutant tested leads to any difference in the K/R-rich or RGRP regions of the AT-hook (Figure 5). However, mutation of BD residues R1433, R1444, and K1451 in the αA helix and ZA-loop leads to chemical shift differences in the C-terminal portion of the AT-hook and the linker (Figure 5). Interestingly, the most extensive differences are observed upon mutation of the linker. Mutation of either the asparagine or prolines in the PNPP leads to extensive localized differences in the chemical shift of residues in the linker and in the

nearby BD αZ helix. In addition, differences are observed in the BD αA and αB helices and the AB loop (Figure 5).

Together, this indicates that the conserved K/R-rich and central RGRP regions of the AT-hook do not make direct contact with the linker or BD but suggests that the C-terminal PAEK element of the AT-hook, containing the conserved EK, is structurally coupled to the linker and BD. In addition, it indicates further coupling between the linker and BD through the AB loop and flanking regions of the αA and αB helices. This is consistent with a hydrogen bond observed in a BRM BD structure between the linker N1379 sidechain and AB loop Y1461 backbone (Figure 3D). Altogether, this analysis supports that the AT-hook, linker, and BD are structurally coupled.

Conserved basic elements in the AT-hook and BD are critical for robust DNA binding

DNA binding was investigated by NMR spectroscopy and/or fluorescence anisotropy (FA) (Figure 6 and Figure Supplementary figure 7 and Supplementary figure 8). Sequential ^{1}H-^{15}N HSQC spectra were collected on ^{15}N-labelled wild-type and mutant proteins upon titration of a 10 bp double-stranded DNA (see methods for sequence). Equilibrium dissociation constants (K_ds) were calculated by plotting chemical shift perturbations (CSPs) as a function of DNA concentration and fitting to a single-site binding model accounting for ligand depletion. For those nearing stoichiometric binding under NMR conditions, FA was used where protein was titrated into fluorescein-labelled 12 bp double-stranded DNA (see methods for sequence).

Wild-type AT-L-BD associated with dsDNA with K_d ~3 μM by NMR and K_d = 8 ± 1 μM by FA (Figure 6), consistent with previously measured K_ds (1.6 ± 0.4 μM[19]). Consistent with a multivalent association, the AT-hook alone and L-BD alone associate more weakly at K_d = 220 ± 30 μM and K_d = 600 ± 200 μM, respectively. Addition of DNA caused significant CSPs in all 7 mutants tested, indicating that all retain some DNA-binding activity (Figure Supplementary figure 9). However, calculated K_ds reveal the relative importance of each conserved element in DNA binding. Mutation of the K/R-rich and RGRP elements of the AT-hook led to a similar decrease in binding to 150 ± 70 μM and 130 ± 30 μM for AT_{GAGGG}-L-BD and AT_{GGGP}-L-BD, respectively. This is consistent with the strong conservation of both elements. Unsurprisingly, binding was further decreased with the charge-reversing mutations in AT_{DGDP}-L-BD to K_d = 410 ± 70 μM. Mutation of the K/R-rich patch in the BD led to similar decreases in affinity to 120 ± 20 μM and 90 ± 20 μM for AT-L-$BD_{3RK/D}$ and AT-L-$BD_{3K\text{-}DNA}$, respectively. Together, this indicates that each of these conserved basic elements is important for robust association of the AT-L-BD module with DNA. In contrast, mutation of the conserved linker PNPP region did not significantly impact affinity for DNA, yielding FA-determined affinities close to wild-type of 11 ± 1 μM and 4 ± 1 μM for AT-L_{PAPP}-BD and AT-L_{ANAA}-BD, respectively. This demonstrates that the conserved linker sequence is not critical to achieve robust binding affinity for DNA.

The conserved linker is important for the conformation of the bound state

To investigate changes in the structural basis of DNA binding, we further analyzed the NMR titrations of the mutants (Figure Supplementary figure 9). Comparison of CSPs between the

apo and DNA-bound states of each mutant reveal a similar binding pocket for all constructs. This consists of the AT-hook, and the ZA-loop and αA helix in the BD, though residues are perturbed to a different extent depending on the mutant. As expected, AT-hook mutants had the most significant CSPs in the BD upon association with DNA. Similarly, BD mutants primarily had CSPs in the AT-hook upon binding to DNA, confirming that the mutations disrupted association of each element with DNA. Notably, only minor CSPs were observed for the AT_{DGDP}-L-BD mutant even in the BD, consistent with the substantially weaker K_d. Linker mutants had CSPs in both the AT-hook and BD upon addition of DNA, revealing that both the AT-hook and BD are binding and consistent with the near wild-type affinities.

To more closely compare the binding mode of each construct, differences in chemical shift between the DNA-bound state of each mutant and the DNA-bound state of wild-type were determined (Figure 7). Interestingly, although mutation of the K/R-rich and RGRP regions of the AT-hook did not affect the BD apo state (Figure 4), the same mutations led to differences in the bound-state chemical shifts of the BD (Figure 7). Likewise, mutations to the K/R-rich patch of the BD led to differences in the bound state of the entire AT-hook. This reveals structural and functional coupling of the two regions in binding to DNA (Figure 7). Moreover, despite not leading to substantial changes in affinity for DNA, mutation of the linker led to substantial chemical shift differences in the bound state of the AT-hook and BD as compared to wild-type (Figure 7). This supports a change in the binding mode of the AT-L-BD upon mutation of the linker and a functional coupling between the linker and both the AT-hook and BD.

To better understand the functional coupling between elements, we further analyzed the differences in chemical shifts between the DNA-bound states of the mutants and wild-type. These can manifest in two manners: 1) differences in the bound state chemical shift that include a different trajectory of CSP, which indicates a unique bound conformation or 2) differences in the magnitude of CSP with no change in trajectory, which indicates a similar bound conformation, but change in the stability of the complex (Figures 8 and 9). Overall, mutation in one of the elements (AT-hook, linker, or BD) primarily leads to differences in the magnitude of the CSPs for the other elements. For example G1369 in the RGRP and A1364 in the K/R-rich region of AT-hook have decreased magnitude of CSP but along the same trajectory upon mutation of either the linker or the BD (Figure 8). This indicates that the interaction of these AT-hook residues with DNA adopt largely the same conformation but are less stabilized upon mutation of the linker or BD. Similarly, S1432 in the ZA loop of the BD has a decreased magnitude of CSP but along the same trajectory upon mutation of the AT-hook or the linker (Figure 8). However, there are a few residues for which unique DNA bound states are observed upon mutation of the adjacent elements. Intriguingly, these include E1374 and K1375 at the C-terminus of the AT-hook and L1376, S1377, and N1379 in the linker (representative residues K1375 and N1379 shown in Figure 9). In addition, K1450 and K1451 in the BD these are highly conserved residues, and in fact in αA helix and Y1440 in the BD ZA-loop adopt a the BD DNA binding pocket, K1451 and Y1440 unique bound state (Figure 9). Notably, all of are the only two highly conserved positions. Together this strongly suggests that the AT-hook, linker, and BD are functionally coupled to achieve optimal DNA binding affinity as well as an optimal conformation in binding to DNA.

Discussion

Together our results reveal that the AT-hook, BD, and short linker between them evolved 930 million years ago and have subsequently been conserved on many Eumetazoan linages. The conservation of all three elements strongly supports functional coupling. NMR analysis of several mutants indeed support that the three elements are structurally and functionally coupled in associating with DNA. In particular, while the AT-hook and BD make multivalent contacts with DNA they are structurally coupled through the linker, which promotes a more stable and unique bound-state conformation. Thus, all three regions of the domain are required to have both optimal binding conformation and binding affinity. Though the mutational analysis here was carried out on the BRM AT-L-BD, the high identity of the AT-L-BD between BRG1 and BRM suggests a nearly identical mode of binding of the BRG1 AT-L-BD (Figure Supplementary figure 1).

The high conservation of the DNA binding pockets strongly supports that this function is important in BAF activity. This is further supported when looking at sites of cancer mutations.[29,30] Conserved residues in the K/R-rich and RGRP elements of the AT-hook as well as K/R residues in the BD basic patch are mutated in BRM and/or BRG1. Intriguingly, the linker is also mutated in cancers. We had previously found that the BRG1 AT-hook and BD span the minor and major grooves in binding to AT-rich DNA.[20] Our computational model of the complex suggested that a turn in the polypeptide at a linker proline (the C-terminal P of the PNPP element) is important for adopting this conformation. Here we find that the full PNPP element is important for promoting the conformation of the AT-L-BD in both the apo and DNA-bound states, and indeed all three prolines in the PNPP element of the linker are seen to be mutated in cancers.[29,30] Prolines are common in non-helical linkers. They can both impart rigidity between linked domains, can make tight turns, and can reduce the conformational independence between linked domains.[31–33] The strong conservation of this element and mutation in cancers suggest that the conformation imparted by the linker is critical for function and that disruption of this conformation may have a deleterious effect on BAF function in disease.

It is not yet clear how the unique conformation of the DNA-bound state manifests in the larger chromatin context. Two recent cryo-EM structures of the BAF complex were solved, each bound to mono-nucleosomes containing either 25 bp or 45 bp of linker DNA.[15,16] Due to conformational dynamics, most of the linker DNA as well as the AT-hook and BD were not resolved. However, by the location of the SnAC domain relative to the nucleosome, the AT-L-BD can be positioned directly adjacent to the entry DNA. Thus, one possibility is that the AT-L-BD associates with the entry DNA and that the bound-state conformation is important in mediating remodeling of the nucleosome, by either altering the conformation and/or dynamics of the DNA. This may be selective for AT-rich DNA, as we have previously found that this module has a moderate preference for AT-rich sequences.[19,20] While not fully explored for the BAF complex, the homologous yeast RSC remodeling complex is known to be stimulated by AT-rich DNA.[34] Similarly, the CHD1 complex activity is stimulated by AT-rich elements, and this is known to be partially due to an AT-hook.[35]

Notably, the activity of the AT-L-BD could be further regulated by post-translational modification. BRG1 and BRM are known to be post-translationally modified, including in and around the AT-L-BD region.[36–38] In particular, the SPN sequence frequently found at the N-terminus of the linker is known to be phosphorylated.[39] The phosphorylation of an SPN element in the CTD of RNA polymerase has been shown to enhance the cis-state of the proline.[40] Our data indicate that phosphorylation of the linker could destabilize the bound-state conformation and thus alter the regulatory role of the AT-L-BD in BAF function.[29,30] Further studies will be required to fully elucidate how this region is regulating BAF activity.

Supplementary Material

Refer to Web version on PubMed Central for supplementary material.

Acknowledgements

Work in the Musselman Lab is funded by the National Institutes of Health (GM128705) and the National Science Foundation (CAREER-1452411). B.L. was funded in part by an Iowa Center for Research by Undergraduates Fellowship. E.A.M. was funded in part by the Iowa Cardiovascular Interdisciplinary Research Fellowship (T32HL007121) and an Arnold O. Beckman Postdoctoral Fellowship. Work in the Harms Lab is funded by the National Institutes of Health (R01GM117140). This project was supported by The Holden Comprehensive Cancer Center at The University of Iowa and its National Cancer Institute Award P30CA086862.

References

1. Yadav T, Quivy J-P, Almouzni G, (2018). Chromatin plasticity: a versatile landscape that underlies cell fate and identity. Science, 361, 1332–1336. 10.1126/science.aat8950. [PubMed: 30262494]
2. Clapier CR, Iwasa J, Cairns BR, Peterson CL, (2017). Mechanisms of action and regulation of ATP-dependent chromatin-remodelling complexes. Nature Rev. Mol. Cell Biol,. 10.1038/nrm.2017.26.
3. Clapier CR, Cairns BR, (2009). The biology of chromatin remodeling complexes. Annu. Rev. Biochem, 78, 273–304. 10.1146/annurev.biochem.77.062706.153223. [PubMed: 19355820]
4. Narlikar GJ, Sundaramoorthy R, Owen-Hughes T, (2013). Mechanisms and functions of ATP-dependent chromatin-remodeling enzymes. Cell, 154, 490–503. 10.1016/j.cell.2013.07.011. [PubMed: 23911317]
5. Blessing C, Knobloch G, Ladurner AG, (2020). Restraining and unleashing chromatin remodelers - structural information guides chromatin plasticity. Curr. Opin. Struc. Biol, 65, 130–138. 10.1016/j.sbi.2020.06.008.
6. Wu JI, Lessard J, Crabtree GR, (2009). Understanding the words of chromatin regulation. Cell, 136, 200–206. 10.1016/j.cell.2009.01.009. [PubMed: 19167321]
7. Alfert A, Moreno N, Kerl K, (2019). The BAF complex in development and disease. Epigenet Chromatin, 12, 19. 10.1186/s13072-019-0264-y.
8. Kadoch C, Hargreaves DC, Hodges C, Elias L, Ho L, Ranish J, Crabtree GR, (2013). Proteomic and bioinformatic analysis of mammalian SWI/SNF complexes identifies extensive roles in human malignancy. Nature Genet, 45, 592–601. 10.1038/ng.2628. [PubMed: 23644491]
9. Kadoch C, Crabtree GR, (2015). Mammalian SWI/SNF chromatin remodeling complexes and cancer: Mechanistic insights gained from human genomics. Sci Adv., 1, 10.1126/sciadv.1500447 e1500447.
10. Mittal P, Roberts CWM, (2020). The SWI/SNF complexin cancer — biology, biomarkers and therapy. Nature Rev. Clin. Oncol, 17, 435–448. 10.1038/s41571-020-0357-3. [PubMed: 32303701]
11. Narayanan R, Tuoc TC, (2014). Roles of chromatinremodeling BAF complex in neural differentiation and reprogramming. Cell Tissue Res, 356, 575–584. 10.1007/s00441-013-1791-7. [PubMed: 24496512]
12. Ronan JL, Wu W, Crabtree GR, (2013). From neural development to cognition: unexpected roles for chromatin. Nature Rev. Genet, 14, 347–359. 10.1038/nrg3413. [PubMed: 23568486]

13. Phelan ML, Sif S, Narlikar GJ, Kingston RE, (1999). Reconstitution of a core chromatin remodeling complex from SWI/SNF subunits. Mol. Cell, 3, 247–253. [PubMed: 10078207]
14. Kadam S, Emerson BM, (2003). Transcriptional specificity of human SWI/SNF BRG1 and BRM chromatin remodeling complexes. Mol. Cell, 11, 377–389. 10.1016/s1097-2765(03)00034-0. [PubMed: 12620226]
15. Mashtalir N, Suzuki H, Farrell DP, Sankar A, Luo J, Filipovski M, D'Avino AR, St R, Pierre AM, Valencia T, Onikubo RG, Roeder Y, Han Y, He JA, Ranish F, DiMaio T, Walz CK, (2020). A Structural model of the endogenous human BAF complex informs disease mechanisms. Cell,. 10.1016/j.cell.2020.09.051.
16. He S, Wu Z, Tian Y, Yu Z, Yu J, Wang S, Li J, Li B, Xu Y, (2020). Structure of nucleosome-bound human BAF complex. Science, 367, 875–881. 10.1126/science.aaz9761. [PubMed: 32001526]
17. Singh M, Popowicz GM, Krajewski M, Holak TA, (2007). Structural ramification for acetyl-lysine recognition by the bromodomain of human BRG1 protein, a central ATPase of the SWI/SNF remodeling complex. ChemBioChem, 8, 1308–1316.10.1002/cbic.200600562. [PubMed: 17582821]
18. Shen W, Xu C, Huang W, Zhang J, Carlson JE, Tu X, Wu J, Shi Y, (2007). Solution structure of human Brg1 bromodomain and its specific binding to acetylated histone tails. Biochemistry, 46, 2100–2110. 10.1021/bi0611208. [PubMed: 17274598]
19. Morrison EA, Sanchez JC, Ronan JL, Farrell DP, Varzavand K, Johnson JK, Gu BX, Crabtree GR, Musselman CA, (2017). DNA binding drives the association of BRG1/hBRM bromodomains with nucleosomes. Nature Commun, 8, 16080. 10.1038/ncomms16080. [PubMed: 28706277]
20. Sanchez JC, Zhang L, Evoli S, Schnicker NJ, Nunez-Hernandez M, Yu L, Wereszczynski J, Pufall MA, Musselman CA, (2020). The molecular basis of specific DNA binding by the BRG1 AT-hook and bromodomain. Biochim. Biophys. Acta Gene Regul. Mech, 1863, 10.1016/j.bbagrm.2020.194566 194566.
21. Delaglio F, Grzesiek S, Vuister G, Zhu G, Pfeifer J, Bax A, (1995). NMRPipe: a multidimensional spectral processing system based on UNIX pipes. J. Biomol. NMR, 6 10.1007/bf00197809.
22. Vranken WF, Boucher W, Stevens TJ, Fogh RH, Pajon A, Llinas M, Ulrich EL, Markley JL, Ionides J, Laue ED, (2005). The CCPN data model for NMR spectroscopy: development of a software pipeline. Proteins, 59, 687–696. 10.1002/prot.20449. [PubMed: 15815974]
23. Johnson M, Zaretskaya I, Raytselis Y, Merezhuk Y, McGinnis S, Madden TL, (2008). NCBI BLAST: a better web interface. Nucleic Acids Res, 36, W5–W9. 10.1093/nar/gkn201. [PubMed: 18440982]
24. Edgar RC, (2004). MUSCLE: multiple sequence alignment with high accuracy and high throughput. Nucleic Acids Res, 32, 1792–1797. 10.1093/nar/gkh340. [PubMed: 15034147]
25. Kumar S, Stecher G, Suleski M, Hedges SB, (2017). TimeTree: a resource for timelines, timetrees, and divergence times. Mol. Biol. Evol, 34, 1812–1819. 10.1093/molbev/msx116. [PubMed: 28387841]
26. Crooks GE, Hon G, Chandonia J-M, Brenner SE, (2004). WebLogo: a sequence logo generator. Genome Res, 14, 1188–1190. 10.1101/gr.849004. [PubMed: 15173120]
27. Ashkenazy H, Abadi S, Martz E, Chay O, Mayrose I, Pupko T, Ben-Tal N, (2016). ConSurf 2016: an improved methodology to estimate and visualize evolutionary conservation in macromolecules. Nucleic Acids Res, 44, W344–W350. 10.1093/nar/gkw408. [PubMed: 27166375]
28. Sanchez R, Meslamani J, Zhou M-M, (2014). The bromodomain: From epigenome reader to druggable target. Biochim. Biophys. Acta,. 10.1016/j.bbagrm.2014.03.011.
29. Cerami E, Gao J, Dogrusoz U, Gross BE, Sumer SO, Aksoy BA, Jacobsen A, Byrne CJ, Heuer ML, Larsson E, Antipin Y, Reva B, Goldberg AP, Sander C, Schultz N, (2012). The cBio cancer genomics portal: an open platform for exploring multidimensional cancer genomics data. Cancer Discov, 2, 401–404. 10.1158/2159-8290.cd-12-0095. [PubMed: 22588877]
30. Gao J, Aksoy BA, Dogrusoz U, Dresdner G, Gross B, Sumer SO, Sun Y, Jacobsen A, Sinha R, Larsson E, Cerami E, Sander C, Schultz N, (2013). Integrative analysis of complex cancer genomics and clinical profiles using the cBioPortal. Sci. Signal, 6, pl1. 10.1126/scisignal.2004088. [PubMed: 23550210]

31. Klein JS, Jiang S, Galimidi RP, Keeffe JR, Bjorkman PJ, (2014). Design and characterization of structured protein linkers with differing flexibilities. Protein Eng. Des. Sel, 27, 325–330. 10.1093/protein/gzu043. [PubMed: 25301959]
32. Chichili VPR, Kumar V, Sivaraman J, (2013). Linkers in the structural biology of protein–protein interactions. Protein Sci, 22, 153–167. 10.1002/pro.2206. [PubMed: 23225024]
33. George RA, Heringa J, (2002). An analysis of protein domain linkers: their classification and role in protein folding. Protein Eng. Des. Sel, 15, 871–879. 10.1093/protein/15.11.871.
34. Lorch Y, Maier-Davis B, Kornberg RD, (2014). Role of DNA sequence in chromatin remodeling and the formation of nucleosome-free regions. Gene Dev, 28, 2492–2497. 10.1101/gad.250704.114. [PubMed: 25403179]
35. Stokes DG, Perry RP, (1995). DNA-binding and chromatin localization properties of CHD1. Mol. Cell. Biol, 15, 2745–2753. [PubMed: 7739555]
36. Bourachot B, (2003). Growth inhibition by the mammalian SWI-SNF subunit Brm is regulated by acetylation. EMBO J, 22, 6505–6515. 10.1093/emboj/cdg621. [PubMed: 14657023]
37. Choudhary C, Kumar C, Gnad F, Nielsen ML, Rehman M, Walther TC, Olsen JV, Mann M, (2009). Lysine acetylation targets protein complexes and co-regulates major cellular functions. Science, 325, 834–840. 10.1126/science.1175371. [PubMed: 19608861]
38. Muchardt C, Reyes JC, Bourachot B, Leguoy E, Yaniv M, (1996). The hbrm and BRG-1 proteins, components of the human SNF/SWI complex, are phosphorylated and excluded from the condensed chromosomes during mitosis. Embo J, 15, 3394–3402. 10.1002/j.1460-2075.1996.tb00705.x. [PubMed: 8670841]
39. Zhou H, Palma SD, Preisinger C, Peng M, Polat AN, Heck AJR, Mohammed S, (2013). Toward a comprehensive characterization of a human cancer cell phosphoproteome. J. Proteome Res, 12, 260–271. 10.1021/pr300630k. [PubMed: 23186163]
40. Lawrence CW, Bonny A, Showalter SA, (2011). The disordered C-terminus of the RNA Polymerase II phosphatase FCP1 is partially helical in the unbound state. Biochem. Bioph. Res. Co, 410, 461–465. 10.1016/j.bbrc.2011.05.160.

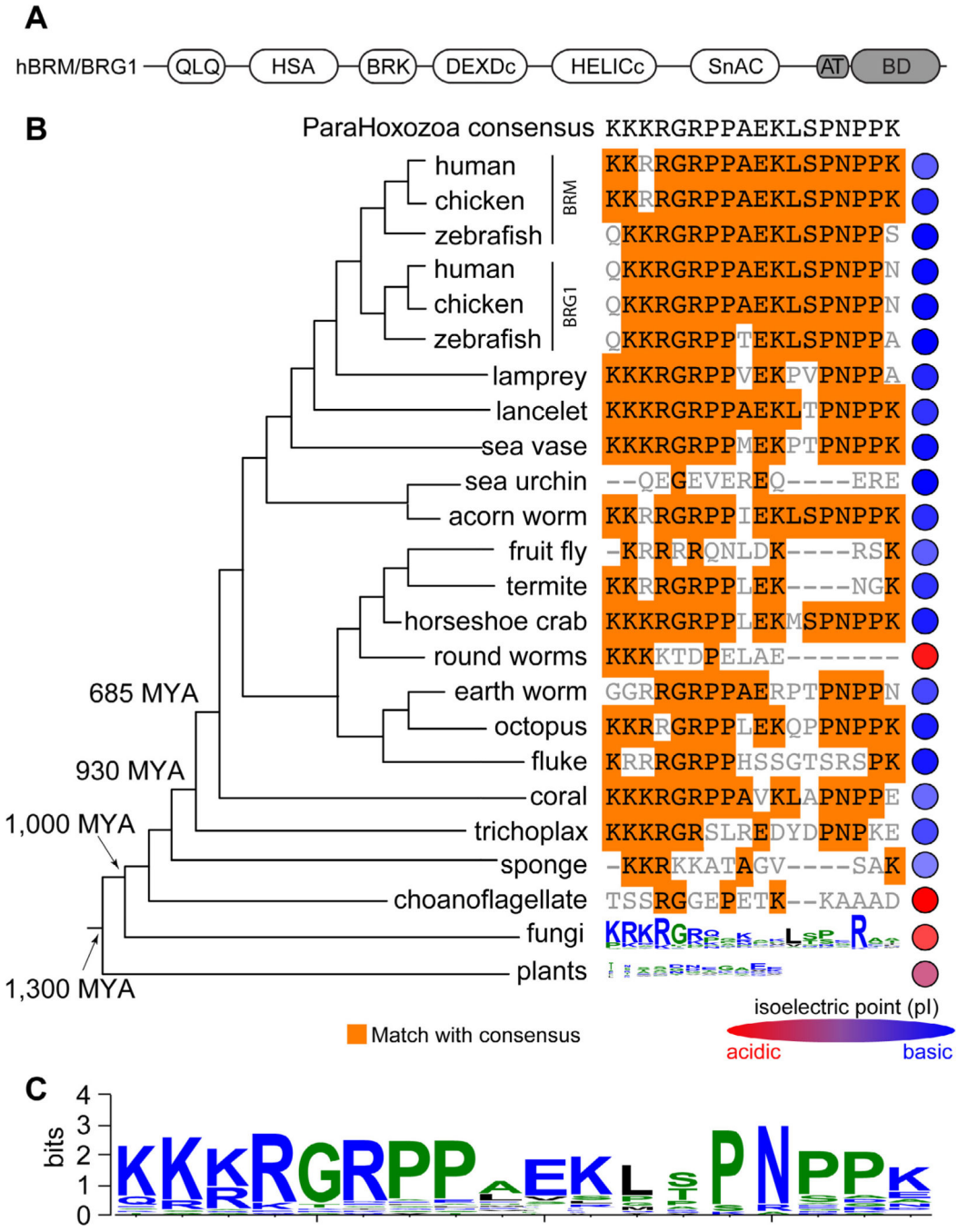

Figure 1.

The BRG1/BRM AT-L-BD DNA binding module is evolutionarily conserved. (A) The domain architecture of the BRG1/BRM ATPase component of the BAF remodeling complex. The C-terminal AT-hook and BD are shaded in grey. (B) Conservation of AT-L-BD DNA binding module across species. The aligned sequence for the region N-terminal to the BD is shown next to each species. The consensus across ParaHoxozoa (humans through Trichoplax) is shown at the top of the tree; amino acids that match the consensus are highlighted in orange. For the fungal and plant clades, the sequence logo for the clade is

shown instead of individual sequences. The circles to the right of the sequences denote the isoelectric point (pI) of the BD, ranging from 4 (bright red) to 7 (purple) to 10 (bright blue). For the fungal and plant clades, the color denotes the average pI over all sequences. The full alignment, scientific organism names, and accession numbers are available in Supplementary Table 1. (C) Sequence logo for the ParaHoxozoa clade.

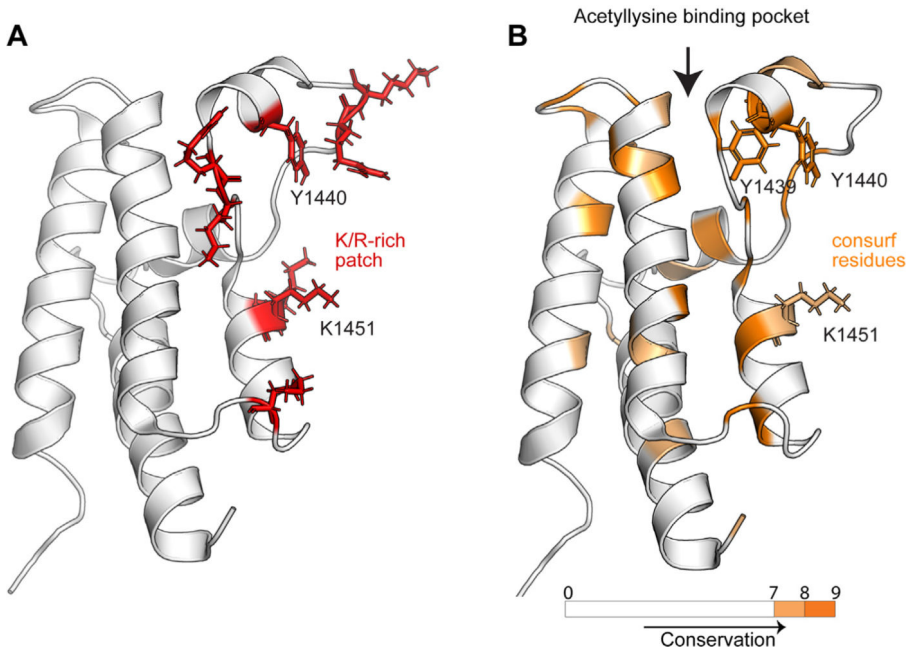

Figure 2.

Conservation of the K/R-rich patch on the BD. (A) Residues forming the K/R-rich patch previously found to be important for DNA binding are shown as sticks highlighted in red on the BRM BD NMR structure (PDB 2DAT). (B) Conserved sites in the ParaHoxozoa clade mapped onto the structure of the human BD (PDB 2DAT) using consurf.[27] Conservation scores range from 0–9 and are color coded from white (score between 0–7), light orange (8), and dark orange (9).

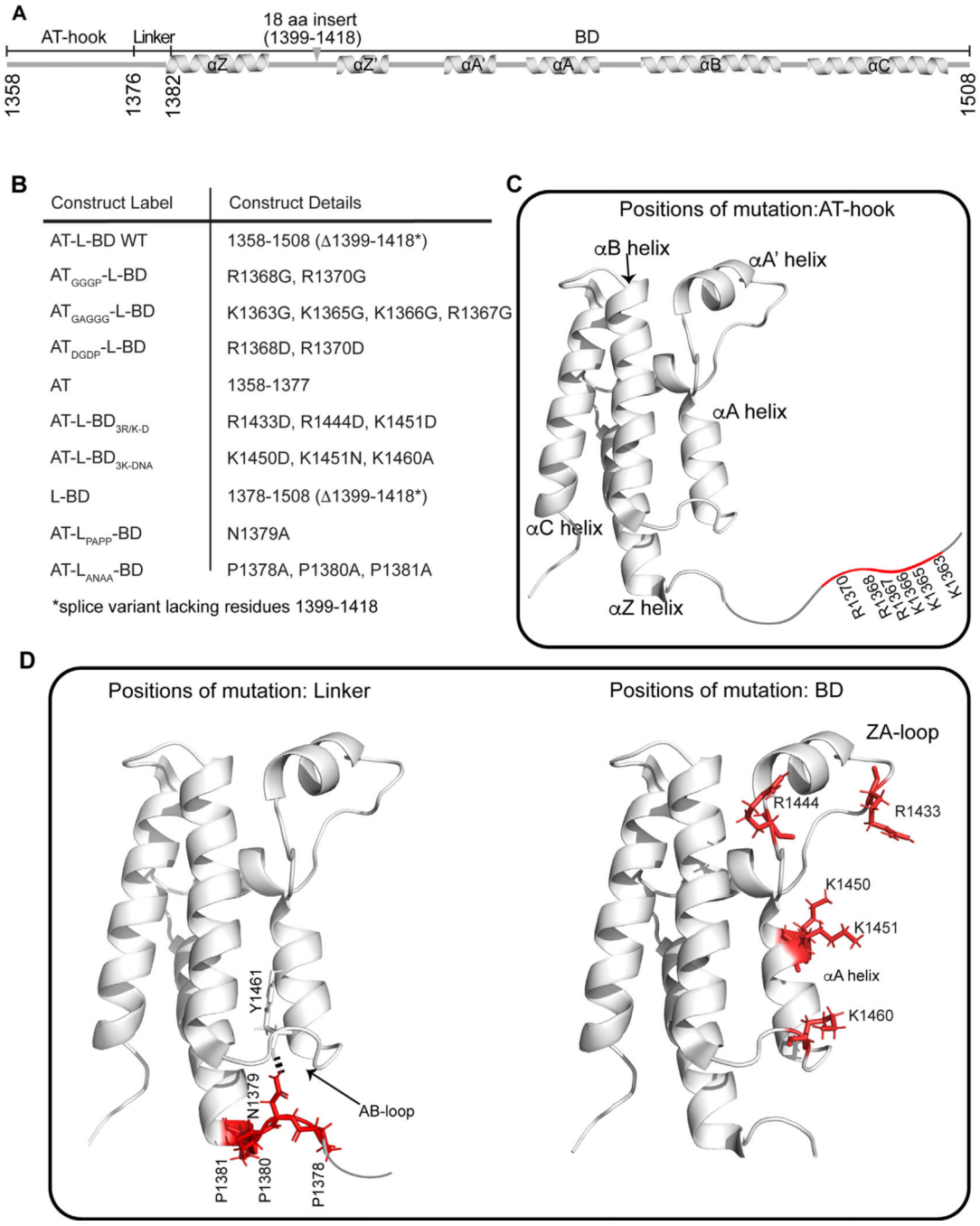

Figure 3.

Mutant constructs of BRM AT-L-BD. (A) Secondary structure of the BRM AT-L-BD. (B) Mutant construct labels and construct details. (C) Residues mutated in the AT-hook are highlighted in red and labelled on the AT-L-BD structure (PDB 2DAT) with the AT-hook drawn in. (D) Residues mutated in the linker (left) and BD (right) are shown as red sticks on the L-BD structure (PDB 2DAT). A hydrogen bond between linker N1379 and AB-loop residue Y1461 is shown as a dashed line.

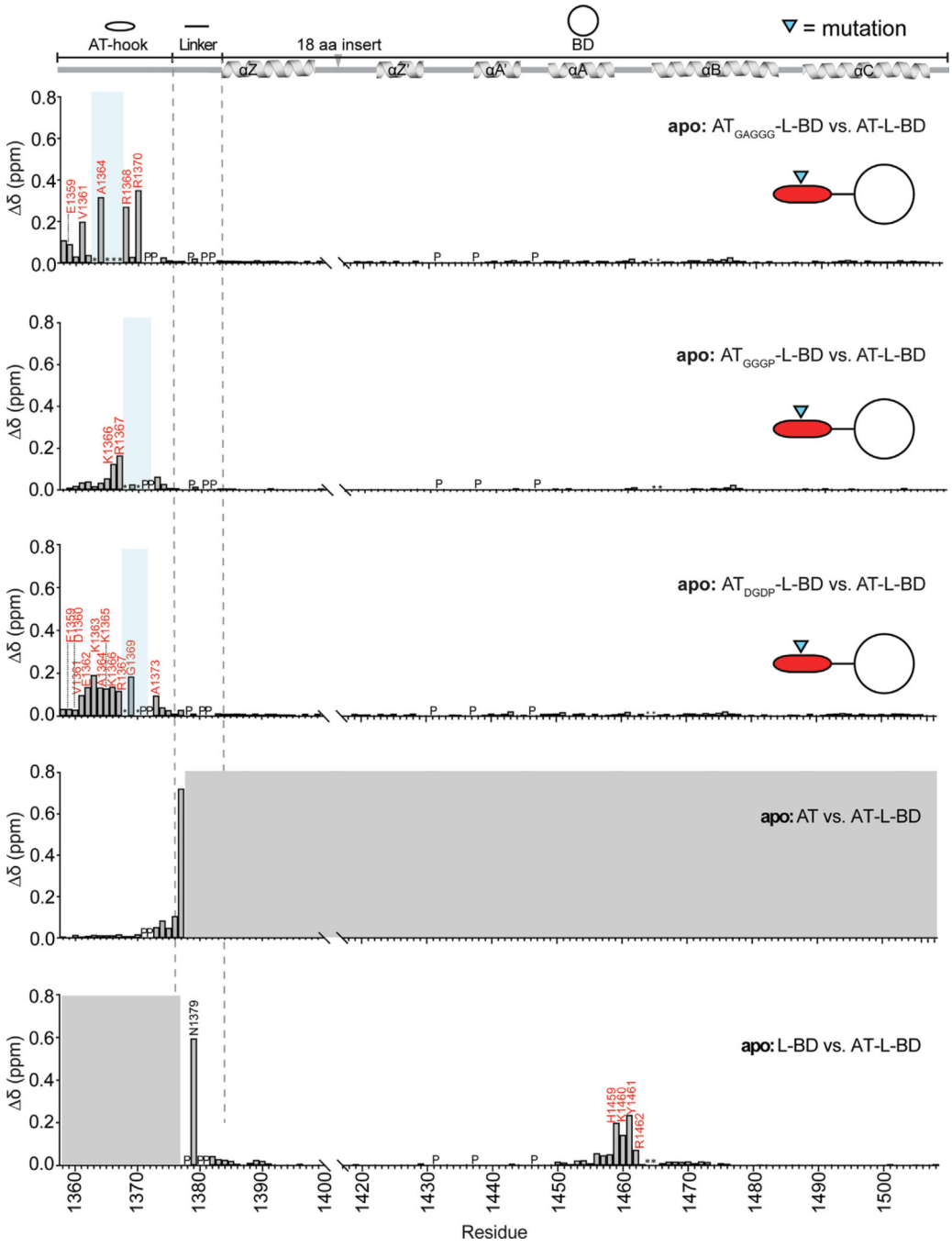

Figure 4.

Mutations in the AT-hook cause localized changes in AT-L-BD. Chemical shift differences (Δδ) are plotted as a function of residue number for wild-type as compared to mutant in the apo states. Bubble diagram of the constructs are denoted in the top right of each plot with the AT-hook represented by an oval bar, the linker by a line, and the BD by a circle. The mutation location is represented by a blue triangle. Mutated residues or regions are shaded in blue on the plots. Residues with significant Δδ are labelled in red and corresponding element(s) shaded in the bubble diagram. Unassigned residues are marked with a (*) and

residues that broaden beyond detection are indicated with an (***). Proline residues are indicated with (P). Residues absent from a given construct are shaded grey. The secondary structure of BRM is indicated above the plots.

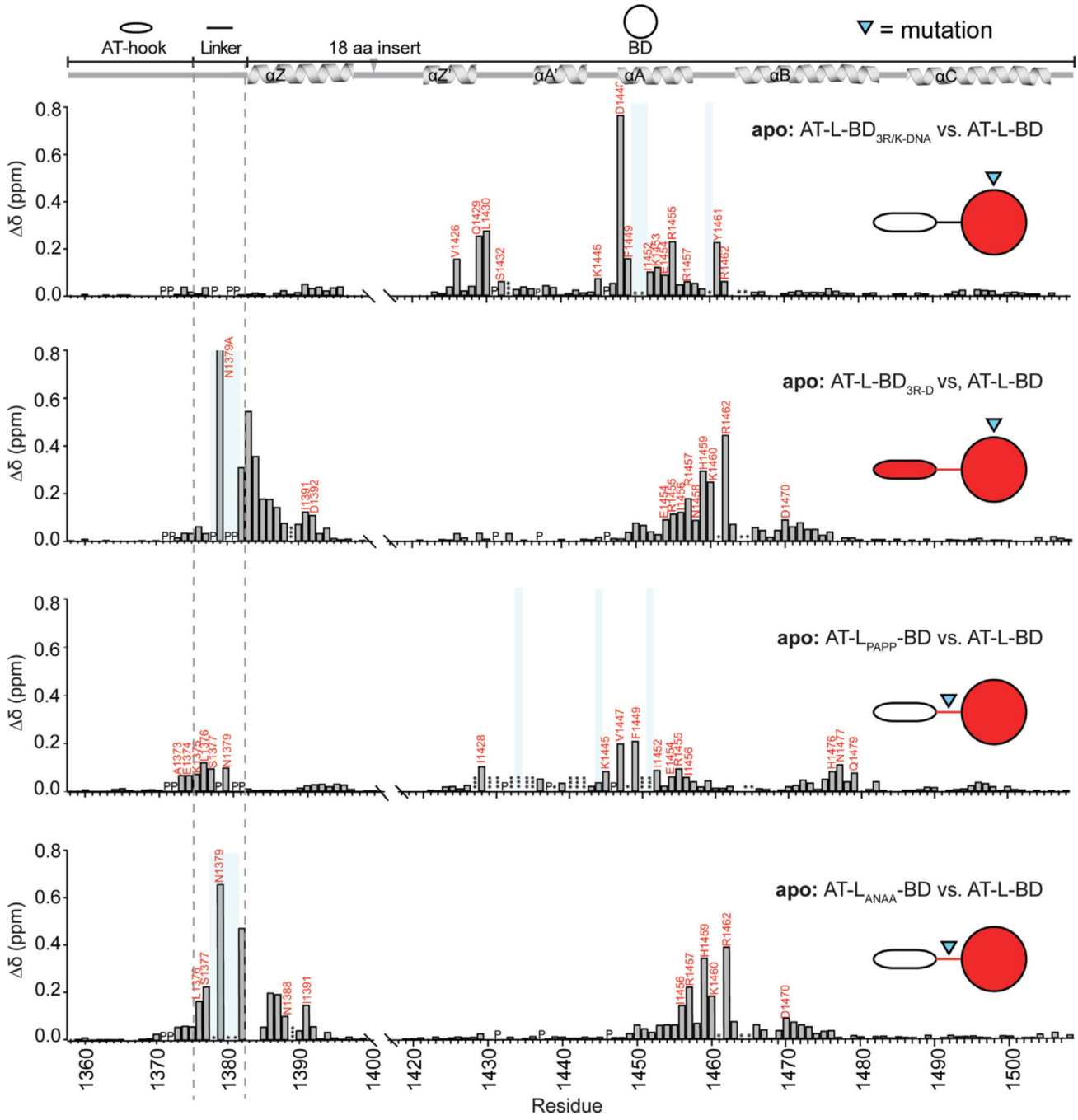

Figure 5.

Mutations in the BD and linker cause localized and disperse changes in AT-L-BD. Chemical shift differences (Δδ) are plotted as a function of residue number for wild-type as compared to mutant in the apo states. Bubble diagram of the constructs are denoted in the top right of each plot with the AT-hook represented by an oval bar, the linker by a line, and the BD by a circle. The mutation location is represented by a blue triangle. Mutated residues or regions are shaded in blue on the plots. Residues with significant Δδ are labelled in red and corresponding element(s) shaded in the bubble diagram. Unassigned residues are marked

with a (*) and residues that broaden beyond detection are indicated with an (***). Proline residues are indicated with (P). The secondary structure of BRM is indicated above the plots.

Construct Label	FA - K_d (μM)	NMR - K_d (μM)
AT-L-BD	8 +/- 1	~3*
AT		220 +/- 30
L-BD		600 +/- 200#
AT_{GGGP}-L-BD		130 +/- 30
AT_{GAGGG}-L-BD	210 +/- 40	150 +/- 70
AT_{DGDP}-L-BD		410 +/- 70
AT-L-$BD_{3R/K-D}$		120 +/- 20
AT-L-BD_{3K-DNA}		90 +/- 20
AT-L_{PAPP}-BD	11 +/- 1	~14*
AT-L_{ANAA}-BD	4 +/- 1	~9*

#Previously determined Morrison et al., Nat. Comm., 2017 [19]
*Shown as approximate as NMR conditions are approaching stoichiometric conditions

Figure 6.

Mutations in the AT-hook and BD decrease affinity for DNA. Binding affinities of WT and mutant AT-L-BD, AT, and L-BD for dsDNA were determined by NMR and/or fluorescence anisotropy titrations. For titrations nearing stoichiometric binding under NMR conditions, the NMR-detemined K_d is listed as an upper-limit and fluorescence anisotropy was used. DNA sequences (of one strand) were 5′-CTCAATTGGT-3′ for NMR and 5′−6-FAM-CCTCAATTGGTC-3′ for fluorescence anisotropy.

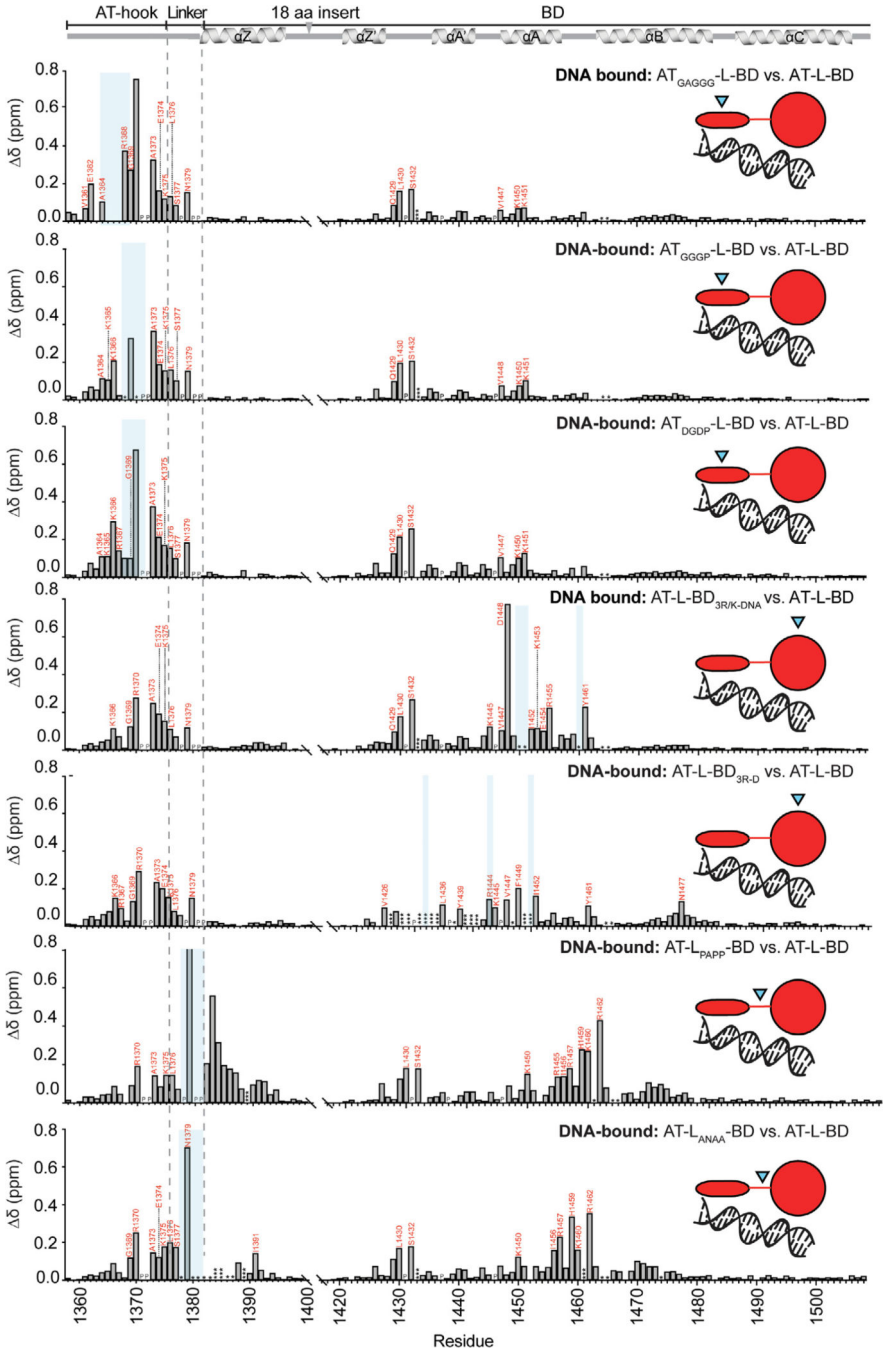

Figure 7.

Mutation of the linker alters the AT-hook and BD DNA binding. Normalized chemical shift perturbations (Δδ) as a function of residue number for wild-type compared to mutant in the DNA-bound state at the highest ratio of AT-L-BD:DNA collected (see Materials and Methods). Bubble diagram of the constructs are denoted in the top right of each plot with the AT-hook represented by an oval bar, the linker by a line, and the BD by a circle. The mutation location is represented by a blue triangle. Residues with significant Δδ are labelled in red and corresponding element (s) shaded in the bubble diagram. Mutated residues or

regions are shaded in blue on the plots. Unassigned residues are marked with a (*) and residues that broaden beyond detection are indicated with an (***). Proline residues are indicated with (P). The secondary structure of BRM is indicated above the plots.

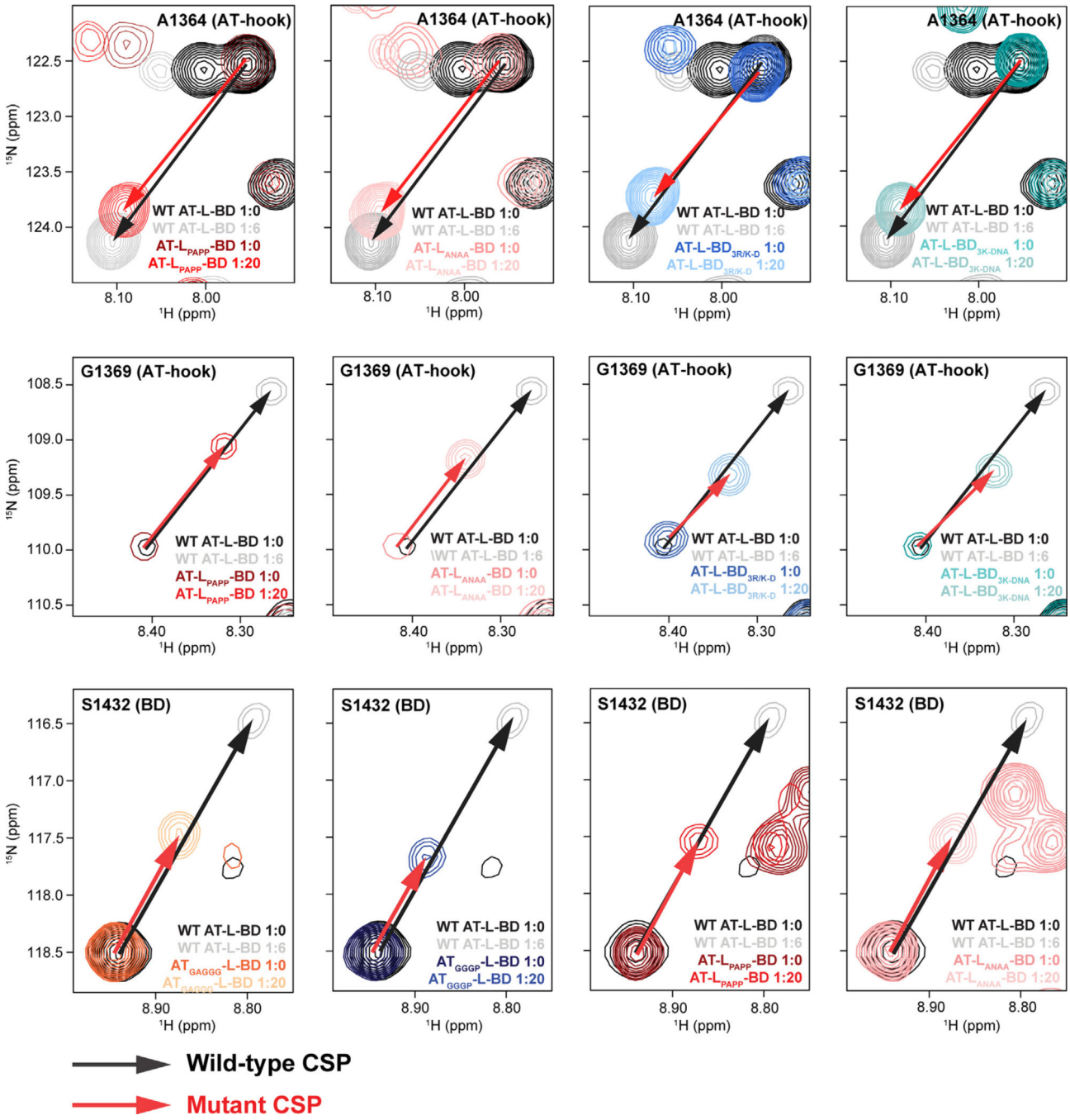

Figure 8.

Mutation primarily changes the magnitude of the CSPs in the AT-hook and BD. CSPs for A1364 in the K/R-rich region of the AT-hook (top), G1369 in the RGRP region of the AT-hook, and S1432 in the BD. Wild-type apo and DNA-bound, and mutant apo and DNA-bound are colored as denoted in legends. Wild-type CSP trajectory is shown with a black arrow and mutant CSP trajectory is shown with a red arrow.

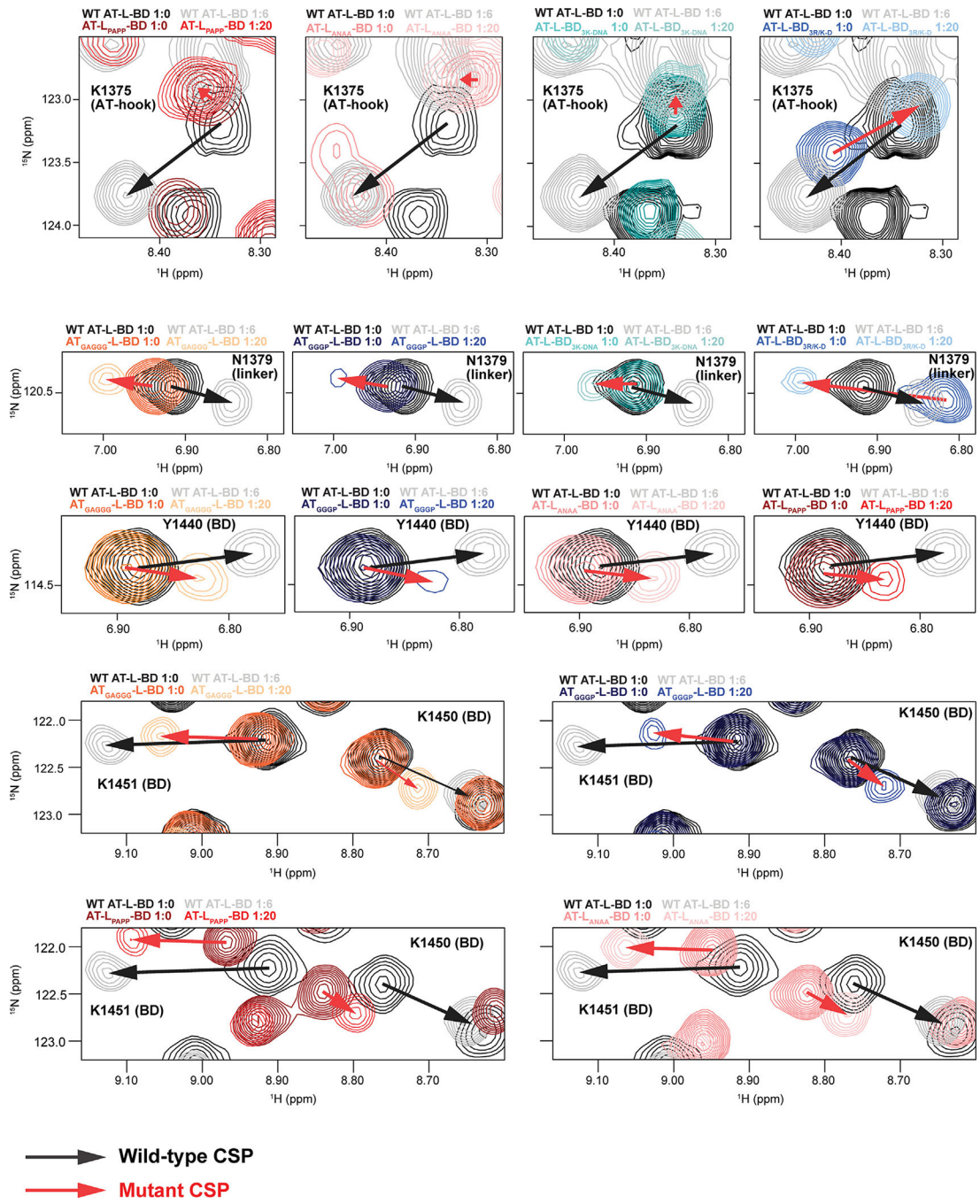

Figure 9.

Upon mutation, select residues adopt a unique DNA-bound conformation. CSPs for K1375 in the C-terminus of the AT-hook (top), N1379 in the linker (middle), and Y1440, K1450, and K1451 in the BD (bottom). Wild-type apo and DNA-bound, and mutant apo and DNA-bound are colored as denoted in legends. Wild-type CSP trajectory is shown with a black arrow and mutant CSP trajectory is shown with a red arrow.